Oxide Particle Surface Chemistry and Ion Transport in "Soggy Sand" Electrolytes

ARTICLE *in* THE JOURNAL OF PHYSICAL CHEMISTRY C · APRIL 2009

Impact Factor: 4.77 · DOI: 10.1021/jp810761e · Source: OAI

2 AUTHORS:

Shyamal Das
Tezpur University
17 PUBLICATIONS **364** CITATIONS
SEE PROFILE

Aninda J. Bhattacharyya
Indian Institute of Science
84 PUBLICATIONS **1,354** CITATIONS
SEE PROFILE

THE JOURNAL OF PHYSICAL CHEMISTRY C

Article

Oxide Particle Surface Chemistry and Ion Transport in "Soggy Sand" Electrolytes

Shyamal K. Das, and Aninda J. Bhattacharyya

J. Phys. Chem. C, **2009**, 113 (16), 6699-6705• Publication Date (Web): 30 March 2009

Oxide Particle Surface Chemistry and Ion Transport in "Soggy Sand" Electrolytes

Shyamal K. Das and Aninda J. Bhattacharyya*

Solid State and Structural Chemistry Unit, Indian Institute of Science, Bangalore 560012, India

Received: December 07, 2008; Revised Manuscript Received: February 19, 2009

The crucial role of oxide surface chemical composition on ion transport in "soggy sand" electrolytes is discussed in a systematic manner. A prototype soggy sand electrolytic system comprising aerosil silica functionalized with various hydrophilic and hydrophobic moieties dispersed in lithium perchlorate−ethylene glycol solution was used for the study. Detailed rheology studies show that the attractive particle network in the case of the composite with unmodified aerosil silica (with surface silanol groups) is most favorable for percolation in ionic conductivity, as well as rendering the composite with beneficial elastic mechanical properties. Though weaker in strength compared to the composite with unmodified aerosil particles, attractive particle networks are also observed in composites of aerosil particles with surfaces partially substituted with hydrophobic groups. The percolation in ionic conductivity is, however, dependent on the size of the hydrophobic moiety. No spanning attractive particle network was formed for aerosil particles with surfaces modified with stronger hydrophilic groups (than silanol), and as a result, no percolation in ionic conductivity was observed. The composite with hydrophilic particles was a sol, contrary to gels obtained in the case of unmodified aerosil, and partially substituted with hydrophobic groups.

1. Introduction

"Soggy sand" electrolytes[1−3] are a new class of soft matter ion conductors comprising dispersions of oxide particles (size: 7−300 nm), such as silica (SiO_2), alumina (Al_2O_3), and titania (TiO_2), in nonaqueous liquid solutions. High ambient-temperature ionic conductivity and beneficial mechanical properties of soft matter make soggy sand electrolytes promising for application in electrochemical devices, such as lithium batteries[4,5] and electrochromic devices.[6−8] The applicability of soggy sand electrolytes in lithium cell assemblies (without any separator) has already been successfully demonstrated.[9,10] Apart from the novelty in terms of applications, soggy sand electrolytes embody a new concept for electrolytes. We discuss this issue with respect to solid polymer electrolytes,[11−13] the most widely studied soft matter electrolytic system. In polymer electrolytes, ion transport is aided by segmental motion of polymer chains, and it has been convincingly demonstrated that ion mobilities are larger in amorphous regions compared to crystalline counterparts. The ionic conductivity of amorphous regions has been shown to be approximately 10^4 times higher than that of the crystalline counterparts.[14] However, in spite of the presence of such high-conducting regimes, the ambient-temperature ionic conductivity of polymer electrolytes are low, $\leq 10^{-6}\ \Omega^{-1}\cdot cm^{-1}$. The highly probable reason is that the volume fraction of amorphous regimes (f) or amorphicity is well below the threshold value for onset in percolation (f_{onset}, left-hand side of Scheme 1a).[14] The $f = f_{onset}$ appears only close to the melting point of the polymer. Therefore, research efforts in improving ambient-temperature ionic conductivity of polymer electrolytes have generally targeted at developing polymeric systems with low degree of crystallinity, that is, systems in the state where $f \geq f_{onset}$ at ambient temperature. In this context, two of the most widely employed approaches that have achieved a reasonable degree of success are (a) composite polymer electrolytes comprising surface-functionalized oxides in a polymer matrix[15,16] and (b) incorporation of nonaqueous molecular liquid solvents to form gel electrolytes.[17,18] Conceptually, the motive behind such material manipulation has been to convert the environment of mobile ions from rigid lattice-like to more liquid-like (right-hand side of Scheme 1a) with the retention of a solid framework at macroscopic dimensions. Generally, such procedures have resulted in enhancement of charge carrier mobilities. It is not clear as to what extent solvation is affected and, hence, the concentration of charge carriers. Coming back to the case of soggy sand electrolytes[1−3] and recently reported plastic-polymer composites,[19,20] the starting material is a liquid electrolyte (including ionic liquids) and aims at the optimization of material properties of liquid electrolytes (left-hand side of Scheme 1b). Optimization procedures should necessarily aim at retaining the high conducting state of liquid electrolytes and at the same time improve other physicochemical properties of liquid systems (right-hand side of Scheme 1b). It is expected that both mobility and concentration of charges will be significantly influenced in the resulting liquid-based composite systems.

SCHEME 1: Representation for Synthesis of Soft Matter Solid Electrolytes (a) with a Higher Fraction of Liquids (Higher Ion Mobility) Regions and (b) from Liquid Electrolytes

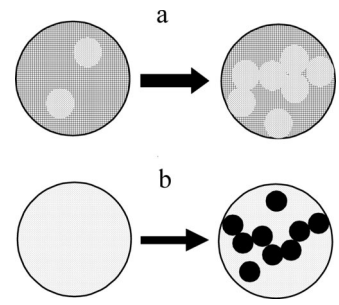

In the published reports[1−3] so far, the ion transport mechanism in soggy sand electrolytes has been qualitatively accounted for

* Corresponding author. E-mail: aninda_jb@sscu.iisc.ernet.in. Phone: +91 80 22932616. Fax: +91 80 23601310.

10.1021/jp810761e CCC: $40.75
Published on Web 03/30/2009

by the concept of heterogeneous doping.[21] The concept of heterogeneous doping was initially developed for the prediction and quantitative description of the beneficial influence of insulator dispersions in weak electrolytes, such as $LiI-Al_2O_3$ and PbF_2-SiO_2. In the case of Al_2O_3 dispersions in LiI, Li^+ ions are adsorbed at the oxide surface, leading to an increased vacancy concentration in the Li sublattice; similarly, in the case of SiO_2 dispersions, the F^- ions are adsorbed at the silica surface, leading to fluorine ion vacancies. In general terms, the undissociated ground state is broken up, and the counter carrier, that is, in this case, vacancy, is set free. In the context of liquid electrolytes, such as Li battery electrolytes, the "ground state" is the undissociated ion pair, which does not contribute to the Li^+ conductivity. Hence, adsorption of the anion (if acidic oxide, such as silica) will lead to dissociation of the LiX ion pair and enhancement of Li^+ ions in the space charge layer in the vicinity of the oxide layer. In refs 2 and 3, it was proposed that, at the silica volume fraction, $\varphi = \varphi_{onset}$, a spanning particle network is formed, resulting in an overlap of space charge and percolation in ionic conductivity. We show here that formation of a connected particle network and space charge is not a sufficient criterion for percolation in ionic conductivity. The surface chemical composition of the oxide particles and their arrangement play a key role in determining the network structure and also percolation in ionic conductivity. It has been recently demonstrated via Monte Carlo computer simulation[22] that temporal stability of the network also plays an important role in percolation of ionic conductivity in soggy sand electrolytes. We systematically highlight the correlation of ion transport with particle network structure in a soggy sand electrolyte system comprising various surface-functionalized aerosil silica dispersed in lithium perchlorate ($LiClO_4$)−ethylene glycol (EG) solutions. The study is implemented via detailed ionic conductivity and rheology (both static and dynamic) measurements. Zeta (ζ)-potential measurements of the oxide surfaces were also done to supplement the findings from ionic conductivity and rheology.

2. Experimental Materials and Methods

Silica Surface Functionalization. For the study, aerosil 300 (Degussa Corporation, hereafter abbreviated as A300) silica was chosen as the starting material. The BET surface area and primary particle size are 300 $m^2\ g^{-1}$ and 7 nm, respectively. The surface of as-received A300 is terminated with hydrophilic silanol (Si−OH) groups with a surface density of 2−3 [−OH] nm^{-2}.[23] Chemical modification of the A300 surface is performed via partial replacement of the silanol groups by suitable hydrophobic/hydrophilic moieties. Functionalization reactions were performed with the following methoxysilanes (MS, all Sigma-Aldrich): methyltrimethoxysilane (MTMS), octyltrimethoxysilane (OTMS), and (3-aminopropyl)trimethoxysilane (APTMS). Appropriate amounts of MTMS, OTMS, and APTMS were added to a stirred suspension of A300 (2 g) in toluene (100 mL) at room temperature (25 °C). The mixture was stirred vigorously for 24 h. The solid phase was recovered by filtration, washed several times with isopropanol and toluene, and then dried at 100 °C for 24 h under vacuum. The dried particles are designated as MA300, OA300, and NA300, corresponding to MTMS-, OTMS-, and APTMS-functionalized A300 silica, respectively. The oxide particles were characterized by Fourier transform infrared (FTIR) spectroscopy (PerkinElmer FTIR Spectrometer Spectrum 1000), transmission electron microscopy (TEM) (FEI Tecnai F30, images are taken at 200 kV), CHN microanalysis (PerkinElmer, 2400 CHNSO system), and thermogravimetric analysis (TGA) (Mettler Toledo).

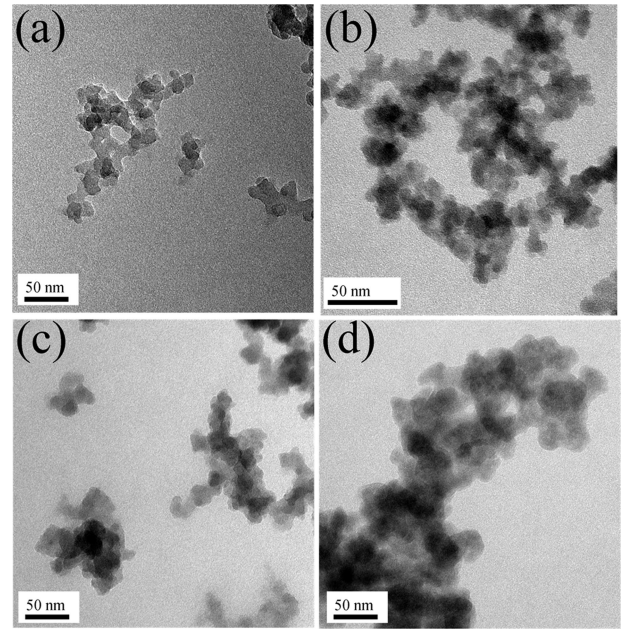

Figure 1. Transmission electron micrographs showing the intrinsic morphology of nonfunctionalized and functionalized aerosil silica particles used in the preparation of soggy sand electrolytes: (a) A300 (as-received), (b) methyl-capped A300 (MA300), (c) amine-capped A300 (NA300), and (d) octyl-capped A300 (OA300).

Electrolyte Preparation. The soggy sand composite electrolytes were prepared by mixing a solution of 0.1 M lithium perchlorate ($LiClO_4$) in ethylene glycol (EG) with nonfunctionalized and functionalized silica particles using a vortex mixture (approximately 2000 vibrations min^{-1}) inside the glovebox. $LiClO_4$ (lithium battery grade, Chemetall) was preheated to 120 °C under vacuum for several days prior to use. EG (Merck) was double-distilled, dried over 4 Å molecular sieves (Qualigens), and stored in the glovebox under pure argon atmosphere (MBraun, water: <0.1 ppm). For electrolyte preparation, A300 and functionalized A300 (i.e., MA300, OA300, NA300) were preheated to 300 and 180 °C, respectively, for 24 h to rule out effects due to physisorped water. The preheat treatment temperatures were selected on the basis of the thermogravimetric analysis (Supporting Information, Figure 1) performed under N_2 atmosphere (heating rate = 5 °C min^{-1}). The weight loss observed for MA300, OA300, and NA300 until approximately 110 °C was due to physisorped water. For temperatures greater than 200 °C, weight loss was significant and this is attributed to decomposition of various surface functional groups. In the case of A300, no significant weight loss was observed in the measuring temperature range (room temperature until 700 °C).

Ionic Conductivity from ac Impedance Spectroscopy. Ionic conductivity was obtained from ac impedance spectroscopy (Alpha, Novocontrol) in the frequency range of $1-10^6$ Hz (amplitude of signal = 0.05 V). The electrolyte was sandwiched between stainless steel electrodes in a home-built cell at room temperature (25 °C). The room-temperature conductivity was evaluated from the intercept of the low frequency spike with the real axis obtained from impedance measurements. The variation in ionic conductivity estimates was approximately ±15%. All preparation and loading of samples into cells for conductivity measurements were performed in a glovebox.

Rheology. Rheological measurements (Advanced Rheometer 2000, TA Instruments) of composite materials under both steady and oscillatory shear were performed to probe the microstructure. Three different test geometries were employed as per

samples and test requirements. The geometries are (a) cone-and-plate, diameter = 20 mm, cone angle = 2°; (b) cone-and-plate, diameter = 40 mm, cone angle = 4°; and (c) parallel plate, diameter = 20 mm. A steady preshear was applied at a shear rate of 0.5 s^{-1} for 60 s, followed by a rest time of 120 s before each dynamic experiment to avoid any previous shear histories and maintain the equilibrium state of the materials.[24] To perform dynamic frequency sweep measurements, the linear viscoelastic (LVE) region for each composite material was first determined by performing a dynamic measurement as a function of strain amplitude at a constant oscillation frequency of 1 rad s^{-1}. All measurements were done at 25 °C.

Surface Potential from the ζ Potential. Surface charge (i.e., potential) was obtained from ζ-potential measurements (Zetasizer Nano ZS, Malvern Instruments). For the ζ potential, a solution of 1 mM $LiClO_4$ in EG was prepared and the silica volume fraction (φ) was adjusted to $\varphi = 0.005$. The basis for selection of salt and oxide concentrations significantly lower than that employed for ionic conductivity and rheology measurements is due to the technical constraints and accuracy involved with electrophoretic measurements.[1−3] The mixture of SiO_2 and $LiClO_4$−EG was stirred and sonicated prior to the measurement to ensure particle nonagglomeration as far as possible.

3. Results and Discussion

Alkoxy Silane Functionalization of A300: Surface Coverage and Particle Size. Elemental analysis and FTIR (Supporting Information, Figure 2) of MA300, OA300, and NA300 indicate successful functionalization of the A300 surface. Estimation of the grafting density of the functional groups shows partial replacement of silanol groups (Si−OH) by various functionalized moieties. The grafting density of the functional groups was obtained using results of the elemental analysis normalized to the surface area (300 m^2 g^{-1}) of as-received aerosil 300. Monolayer coverage of the functional moieties with no alkoxy groups retained on the silica surface (A300) was assumed for the calculation of the density of various functional groups. Among the various alkoxy-silane-functionalized silica samples, NA300 showed the highest surface loading. Estimations revealed approximately 78% coverage (grafting density = 2.4 nm^{-2}) of the surface by the amino functional group. This is attributed to the fact that hydrolysis of silanol (Si−OH) groups[25] is considerably enhanced due to the presence of strongly basic amino groups in nonaqueous medium. The estimated percentage coverage of the grafted octyl group (OA300) (grafting density = 1.7 nm^{-2}; coverage = 56%) is lower compared to that of the methyl group (MA300) (grafting density = 2.0 nm^{-2}; coverage = 67%). As the octyl group is relatively large, once it is grafted to the surface, it provides a steric barrier, preventing solvent molecules carrying octyl moieties to get access to the unmodified silica surface.

TEM images of A300, along with MA300, OA300, and NA300, are shown in Figure 1. All functionalized silica samples show branched aggregates or agglomerates similar to those of A300.[23] This suggests that surface functionalization of A300 with various alkoxy silanes employed here did not affect the intrinsic morphology of A300. Such consistency in the microstructure is extremely beneficial for the present study, which focuses on correlation of network morphology with ion transport. However, as can be observed from the TEM images, the primary particle size of MA300, OA300, and NA300 increases (i.e., surface area decreases) due to grafting of large molecules on the silica surface. According to particle size (estimated using TEM), they can be arranged as follows: A300 (7−10 nm) ≤ MA300 (7−12 nm) < NA300 (20−25 nm) < OA300 (25−30 nm).

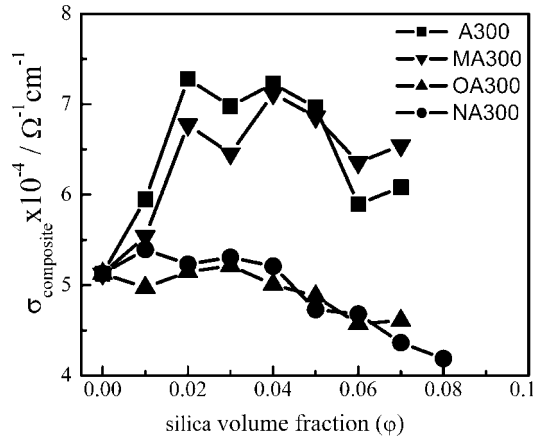

Figure 2. Variation of effective composite (0.1 M $LiClO_4$−EG/aerosil−SiO_2) ionic conductivity as a function of silica volume fraction (φ) at 25 °C, as obtained from ac-impedance spectroscopy: A300, as-received; MA300, methyl-capped A300; NA300, amine-capped A300; and OA300, octyl-capped A300.

Ionic Conductivity as a Function of Surface Hydrophobicity/Hydrophilicity and Oxide Volume Fraction. Figure 2 shows the room-temperature (25 °C) effective composite ionic conductivity as a function of silica volume fraction (φ) for various composites. The variation in ionic conductivity versus silica volume fraction strongly depends on the surface chemical composition of the silica particles. In the case of A300 and MA300, ionic conductivity exhibits a percolation-type behavior very similar to that of composite materials with interfacial ion conduction.[21,26,27] The ionic conductivity initially increases with the increase in silica volume fraction (onset percolation threshold, $\varphi_{onset} \ll 0.01$), reaches a maximum, and then decreases after the maximum. Ionic conductivity increases from 5.1 × 10^{-4} $\Omega^{-1}\cdot cm^{-1}$ for 0.1 M $LiClO_4$−EG by approximately 1.4 times to 7.2 × 10^{-4} $\Omega^{-1}\cdot cm^{-1}$ (φ_{max} = 0.02−0.05) for both A300 and MA300. The conductivity at $\varphi = 0.07$ for A300 and MA300 is approximately 6.3 × 10^{-4} $\Omega^{-1}\cdot cm^{-1}$, still higher than the ionic conductivity of the nonaqueous 0.1 M $LiClO_4$−EG solution. Due to technical constraints (maximum rotation speed of the vortex mixture being approximately 2000 vibrations min^{-1}) in the preparation of composite samples with higher amounts of A300 or MA300, it would be difficult to comment on the existence of an offset percolation threshold ($\varphi = \varphi_{offset}$), that is, the concentration of A300 or MA300 at which composite ionic conductivity is lower than that of nonaqueous 0.1 M $LiClO_4$−EG solution. Due to the difficulty in obtaining homogeneous samples for $\varphi > 0.07$, we do not discuss this issue any further (homogeneity was ascertained via visual observation of the degree of silica wetting by the nonaqueous solution). Unlike the A300 and MA300 composites, no percolation-type behavior in ionic conductivity is observed for the OA300 and NA300 composites. Dispersion of OA300 and NA300 in 0.1 M $LiClO_4$−EG does not result in any significant enhancement of ionic conductivity, and for $\varphi \geq 0.04$ ($=\varphi_{offset}$), the effective composite conductivity is lower than the solution conductivity and also decreases gradually with an increase in φ.

The ionic conductivity in the various silica composites can be accounted for on the basis of both particle arrangement and heterogeneous doping. Silica, being an acidic oxide (pH of zero charge (pzc) in aqueous medium ~3[28]), typically traps ClO_4^- anions on the surface resulting from the breakup of ion pairs

($Li^+\cdots ClO_4^-$) in the nonaqueous solution. This is confirmed via measurement of a negative ζ potential (ζ potential $= -2.5$ mV) for the as-received silica material, that is, A300. The trapping of anions on the silica results in a space charge layer (Debye length, $\lambda \sim 0.6$ nm, assuming $K_a = 6$ Lmol^{-1} at 25 °C[29]) in the vicinity of the oxide containing a high concentration of the counterion Li^+ (compared to the bulk electrolyte). The system percolates, that is, becomes conducting only at a particular concentration of silica, referred to as the onset percolation threshold ($\varphi = \varphi_{onset}$). At $\varphi = \varphi_{onset}$, an attractive particle network spanning macroscopic dimensions of the electrolyte is formed (Figure 4). In the case of the A300 composite, the particle network is held together via interaction between the silanol groups of neighboring particles. Due to the close proximity of the particles, the space charge layers are expected to overlap, leading to a facile pathway for Li^+ ions. The ionic conductivity increases with the increase in silica volume fraction until the appearance of a maximum in conductivity at a particular silica volume fraction, φ_{max}. The increase in ionic conductivity with the silica volume fraction is attributed to the fact that the number of possible pathways for Li^+ ion conduction increases with oxide addition, with the number being maximum at $\varphi = \varphi_{max}$. Beyond $\varphi = \varphi_{max}$, the ionic conductivity starts decreasing, and at $\varphi \geq \varphi_{offset}$, the composite conductivity becomes lower than that of the nonaqueous solution of 0.1 M $LiClO_4$−EG [as remarked earlier, φ_{offset} could not be observed in the case of A300 and MA300 due to technical constraints in preparing samples with $\varphi > 0.07$]. The decrease in conductivity after the maximum is attributed to the blocking of percolating pathways. Very close proximity of the particles leads to probable elimination of the high conducting space charge layer around the particles. This scenario is similar to that of particles being in contact with each other. Offset in percolation may also result from instability of the particle network, as shown recently in ref 22.

The trapping efficiency and nature of trapped species are severely influenced by chemical functionalization of the surface. As discussed earlier, functionalization procedures employed here with various silane moieties result in partial replacement of surface silanol groups. For MA300 and OA300, ClO_4^- anion trapping takes place, but to a much lesser degree compared to A300. The hydrophobic alkane chains arrange close to the silica surface and provide a steric barrier for the Li^+ motion. In the event of formation of an attractive particle network (via van der Waals interaction), percolation of Li^+ ions (and, hence, enhancement in ionic conductivity) through the network depends heavily on the alkane chain length. Whereas Li^+ ions can still percolate in the MA300 composite, the octyl chains completely block Li^+ ion motion in the particle network, and as a result, no enhancement in ionic conductivity is observed. In the case of NA300, Li^+ ions are adsorbed instead of ClO_4^-. This is confirmed via measurement of a positive ζ-potential voltage (+0.30 mV). Percolation in conductivity does not take place in the NA300 composite due to unstable network formation. In the subsequent section, we discuss the particle network based on rheology results and its correlation with ion transport.

Steady-State and Dynamic Rheology of Various Composites. Static and dynamic rheology tests were performed to investigate particle arrangement in the composite electrolytes. Photographs depicting the physical appearance at room temperature of various composite electrolytes are shown in Figure 3. For all composites, the silica volume fraction (φ) is equal to 0.07, which is also the highest silica concentration used for the ionic conductivity measurement. A300 (Figure 3a) and OA300 (Figure 3b) show gel formation, whereas no gel formation was observed for NA300 (Figure 3d) even at $\varphi = 0.07$. Though the appearance of MA300 (Figure 3c) resembles that of a viscous fluid, we show later (via rheology) that gelation also takes place in the case of MA300. Figure 4 shows the variation of viscosity (η) as a function of shear rate ($\dot{\gamma}$) for all composites at $\varphi = 0.07$. A300 and OA300 show shear thinning; that is, macroscopic viscosity decreases with an increase of shear rate. Contrary to the optical appearance, MA300 also shows the phenomenon of shear thinning. Shear thinning behavior is possible if and only if the silica particles form an attractive network. Fitting the plots to the power law equation, $\eta = m\dot{\gamma}^{(n-1)}$, shows that $n < 1$, which implies the existence of a composite microstructure comprising a network of particles.[30] Whereas the zero shear viscosities of A300 and OA300 are almost the same (equal to approximately 400 kPa·s), the zero shear viscosity for MA300 is 10 kPa·s. There is a 40-fold decrease in zero shear viscosity in MA300, and this accounts for the viscous fluid-like visual observation. The reason for exhibiting shear thinning behavior in A300, OA300, and MA300 is primarily due to rupture of the attractive network into smaller and smaller connective flow units (smaller portions of the attractive particle network, which contain a number of connected particles). Since the flow units also contain nonaqueous liquid, the volume of which is proportional to the size of the flow unit, breaking of the flow unit into smaller units releases this liquid in which the flow units can move. With increasing shear rates, the size of the flow units decreases, thus releasing more and more liquid. Ultimately, at very high shear rates, the flow unit is the particle itself. At such shear regimes, the viscosity becomes identical to that of a slurry where the particles are highly repulsive. The nonexistence of any kind of attractive network can be observed only in the case of NA300, where η is almost independent of γ,˙ resembling a Newtonian fluid. Though it appears that there is a minor shear thinning behavior, however, η is low (0.05−0.3 Pa·s) and very similar to η of ethylene glycol (=0.02 Pa·s at 25 °C[31]). The slight increase can be attributed to the combined effects of added salt and silica.

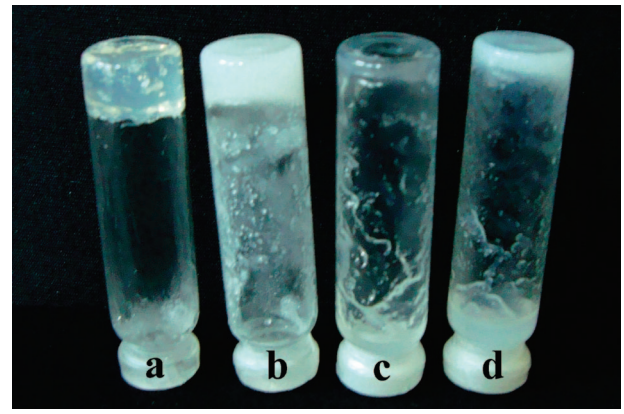

Figure 3. Photographs showing the visual appearance of various composite electrolytes: (a) A300 (as-received), (b) octyl-capped A300 (OA300), (c) methyl-capped A300 (MA300), and (d) amine-capped A300 (NA300). For all composites, the silica volume fraction (φ) = 0.07.

Dynamic rheology measurements were performed to further probe the composite microstructure. The experiments were performed under constant strain, the magnitude of which was within the linear viscoelastic regime. Figure 5 shows the frequency dependence of elastic (G') and viscous (G'') moduli for all composite electrolytes. Over the measured frequency range, G' is greater than G'' for the A300, OA300, and MA300

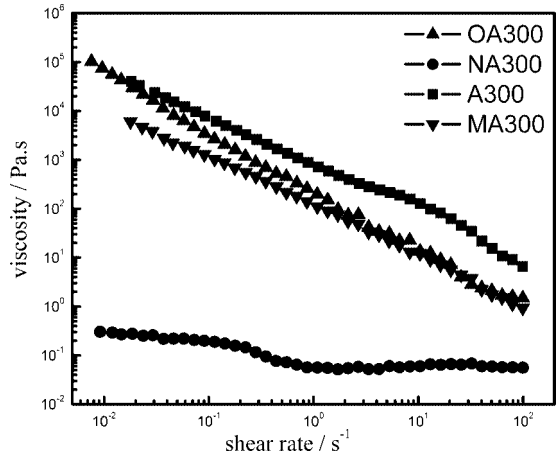

Figure 4. Steady-shear viscosity as a function of shear rate for various composites: A300, as-received; MA300, methyl-capped A300; NA300, amine-capped A300; and OA300, octyl-capped A300. For all composites, the silica volume fraction (φ) = 0.07.

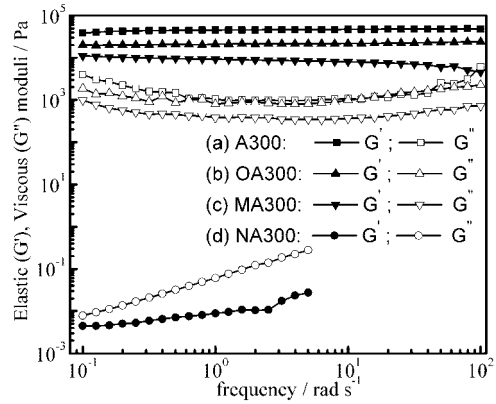

Figure 5. Variation of elastic (G') and viscous (G'') moduli as a function of frequency for various composites, as obtained from dynamic frequency sweep measurements: A300, as-received; MA300, methyl-capped A300; NA300, amine-capped A300; and OA300, octyl-capped A300. For all composites, φ = 0.07.

samples. Barring small deviations, as observed in the case of G'', both moduli are fairly independent of frequency. $G' > G''$ suggests that dispersion of A300, OA300, and MA300 in EG−$LiClO_4$ results in a composite electrolyte with intrinsic elasticity. The degree of elasticity is a function of the surface functional group. At 1 rad s^{-1}, G' equals 45, 21, and 9 kPa, respectively, for A300, OA300, and MA300. The favorable mechanical property of the A300 composite has already been demonstrated to be beneficial for lithium batteries. In refs 9 and 10, it was shown that, in a lithium battery with $LiPF_6$/$LiCF_3SO_3$ in EC−DMC/A300, soggy sand electrolytes can be assembled without any conventional separator material. The frequency-independent response of both moduli also demonstrates the stability of the composites over a wide range of time scales. This strongly suggests that A300, OA300, and MA300 composites are physical gels where silica particles are interconnected via physical bonds to form a space-filling network structure.[24,30,32] In contrast to A300, OA300, and MA300, for the NA300 composite, G'' is greater than G' and both moduli display strong frequency dependence in the measured frequency range. The viscous liquid-like behavior of NA300 is, thus, also reflected from the dynamic rheology experiment. The NA300 composite resembles a sol consisting of nonflocculated silica units.[33] Thus, the findings from dynamic rheology experiments are consistent with those from steady-state experiments for all composites.

We discuss now in greater detail the particle network and its correlation with ion transport. The chemical composition of the silica particle surface solely determines the macroscopic mechanical consistency of the composites. A gel composite electrolyte, as in the case of A300, OA300, and MA300, results essentially from the formation of an attractive particle network spanning the electrolyte. Absence of such a spanning particle network leads to a composite with the consistency of a viscous liquid or sol, as observed in the case of the NA300 composite. The percolating network may originate from an arrangement of particles touching one another within van der Waals range or particles residing very close to each other in the regime of overlapping space charges. An attractive network solely due to overlap of the space charge layer can be ruled out as attraction of two equally charged silica particles in the case of a symmetric AB salt is not possible.[34] Network formation via space charge overlap is more probable in the case of salts with higher valency of the type, AB_2, and so forth, where charge ordering may lead to an attraction. We interpret the formation of a particle network in A300, OA300, and MA300 composites in terms of van der Waals forces or chemical (covalent) bonding.

The different kinds of colloidal interactions prevailing in the composite systems are depicted in Scheme 2. In the case of A300, which shows gel behavior even at low silica concentrations ($\varphi \geq 0.02$), there are two possibilities for the formation of a spanning attractive particle network. The silanol (Si−OH) group present on A300 interacts via hydrogen bonding either with solvent molecules or with the silanol group of adjacent silica particles. In this context, the chemical nature of the solvent is highly significant. In the case of a highly polar solvent, the solvent molecules organize in the vicinity of silica particles, possibly via hydrogen bonding with the silanol groups on the silica surface. The layer of solvent molecules (or solvation layer) provides short-range repulsive forces between silica particles, resulting in sol morphology. On the other hand, due to negligible interaction between solvent molecules and surface silanol groups, no solvation layer exists in the case of nonpolar solvent. At sufficiently high silica concentration, the driving force for formation of a three-dimensional network of particles is via hydrogen bonding between surface silanol groups of adjacent silica particles.[35−39] The existence of the particle network results in a colloidal gel. The existence of a three-dimensional network based on visual appearance and static and dynamic rheology of the composite comprising hydrophilic A300 in polar ethylene glycol (ε = 37.7)−$LiClO_4$ solution contradicts the propositions suggested in literature. We envisage that the interaction between surface silanol groups of adjacent silica particles (Scheme 2a) dominates over the solvent−surface interaction, thus leading to gel morphology. It is highly probable that the solvent molecules coordinate with the salt ions, resulting in reduced interaction with silica surface silanols. The interaction of the remaining free silanols on the silica surface breaks the ion pairs and adsorbs anions (X^-) on the surface. This results in an increase in the concentration of free cations (M^+) in the vicinity of the silica surface. At a silica concentration equal to the onset percolation threshold, a percolating particle network is formed, and excess cations in the space charge layer can percolate freely through this network, resulting in enhancement of ionic conductivity compared to that of the nonaqueous salt solution. At the offset percolation threshold, blockage of percolation pathways occurs due to particles being in contact. The microstructure of OA300 and MA300 can be explained on the basis of van der Waals interaction, as shown in Scheme 2b,c. Both

SCHEME 2: Representation of Various Interactions Prevailing in the Composite Systems: (a) A300, (b) MA300, (c) OA300, and (d) NA300

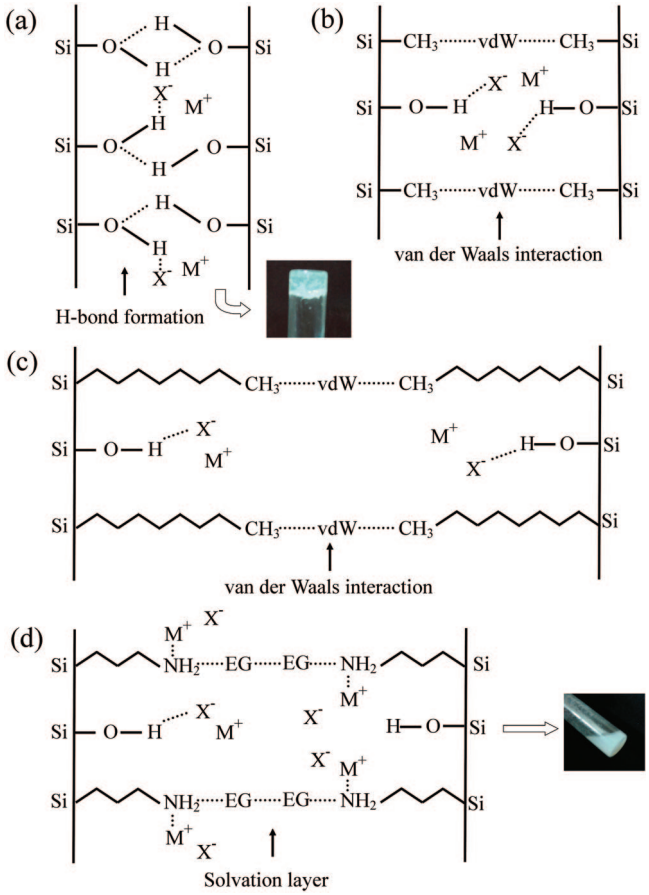

composites comprise silica particles with the surface being predominantly hydrophobic in character. To understand the magnitude of van der Waals forces between hydrophobic silica particles, we estimated the Hamaker constant (A_{eff}).[24,31,40−43] A_{eff} is found to be $\sim 10^{-21}$ J for both OA300 and MA300. This is typical for van der Waals interactions of a nonpolar medium across a polar solvent.[24,31,40] Visual appearance and rheology signify that the magnitude of the interaction between silica particles tethered with a small methyl group is appreciably lower than between those with the long octyl group (zero shear viscosity and elastic modulus for MA300 is lower than those for OA300). This is probably the reason why the MA300 gel falls apart under gravity (Figure 3c). Ionic conductivity of the composite electrolytes is also dependent on the tethered alkane chain length. In spite of a higher number of residual silanols in OA300 ([OH] = 44%) in comparison to MA300 ([OH] = 33%), no conductivity enhancement is observed in the case of OA300 compared to MA300. This is attributed to the conformation adopted by the tethered octyl chains. The tethered nonpolar chains are expected to remain close to the silica surface, forming a dense layer, thus preventing interaction of the surface silanols with the solvent molecules, as well as with the surface silanols from the adjacent silica particles.[44−48] Though the free silanols present on the OA300 surface adsorb anions (ζ potential = −2.03 mV), the dense hydrophobic layer provides a steric barrier to the movement of free cations (M^+), resulting in nonpercolative ion transport in spite of the existence of a spanning particle network. As the small methyl groups are less effective as steric barriers to ion movement compared to the octyl groups, enhancement in ionic conductivity is observed in the case of MA300 (ζ potential = −1.77 mV). The ζ-potential values are quite consistent with the density of silanol groups. As depicted in Scheme 2d, the solvation layer plays the key role in sol formation in the case of NA300.Due to the strong polar nature of the tethered amino propyl group, the solvent molecules, which are also strongly polar, instantaneously organize themselves in the vicinity of the silica surface. Therefore, a solvation layer is expected to cover up the silica particles. Nonflocculation of silica particles occurs due to a short-range repulsive force that arises from the solvation layer. These stable nonflocculated silica units form the sol in NA300, similar to what has been already reported in literature.[49−52] There is no enhancement in ionic conductivity in NA300 due to adsorption of cations (M^+) by the amine groups. The measured ζ potential for NA300 was found to be +0.276 mV, suggesting adsorption of positive charge on the silica surface.

4. Conclusions

We have discussed here in detail the importance of the particle network in determining both ion transport and mechanical strength of soggy sand electrolytes, a promising lithium battery soft matter electrolyte. The nature, strength, and extent of interaction between the neighboring particles or particles and solvent is mainly controlled by the particle surface chemical moieties and, to a certain extent, the properties of the solvent. Although spanning the dimensions of the network of electrolytes is a prerequisite, our studies reveal that steric hindrance from the surface chemical moiety is detrimental and should be substantially low for percolation in ion transport to take place. We believe that the present study will, in general, help in the fundamental understanding of ion transport in hybrid electrolytes, as well as optimization of their physicochemical properties for various electrochemical applications, especially lithium batteries.

Acknowledgment. The authors thank the Indian Institute of Science (IISc.), Bangalore, for financial assistance; I.S. Jarali for TGA and FTIR; and Amit Mondal (INI-IISc., Bangalore) for TEM. We also thank S. Balakrishnan and N. Gopalakrishnan, of TA Instruments, Bangalore, for rheology measurements; Vikas Rane, Evonik, India, for aerosil samples; and AIMIL Ltd., Bangalore, for the zeta-potential measurements. The authors also thank J. Maier, MPI-FKF, Stuttgart, Germany, for useful discussions.

Supporting Information Available: Thermogravimetric analysis (TGA) and Fourier transform infrared (FTIR) spectroscopy of various aerosil particles employed for preparing the composites. This material is available free of charge via the Internet at http://pubs.acs.org.

References and Notes

(1) Bhattacharyya, A. J.; Maier, J. *Adv. Mater.* **2004**, *16*, 811.
(2) Bhattacharyya, A. J.; Maier, J.; Bock, R.; Lange, F. F. *Solid State Ionics* **2006**, *177*, 2565.
(3) Edwards, W. V.; Bhattacharyya, A. J.; Chadwick, A. V.; Maier, J. *Electrochem. Solid-State Lett.* **2006**, *9*, A564.
(4) Bruce, P. G.; Scrosati, B.; Tarascon, J. M. *Angew. Chem., Int. Ed.* **2008**, *47*, 2930.
(5) Guo, Y.-G.; Hu, J.-S.; Wan, L.-J. *Adv. Mater.* **2008**, *20*, 2878.
(6) Niklasson, G. A.; Granqvist, C. G. *J. Mater. Chem.* **2007**, *17*, 127.
(7) Choy, J. H.; Kim, Y. I.; Kim, B. W.; Park, N. G.; Campet, G.; Grenier, J. C. *Chem. Mater.* **2000**, *12*, 2950.
(8) Duluard, S. New Polymer Electrolytes Membranes Based on Lithium Conductive Ionic Liquids for All Plastic Flexible Eletrochromic Devices. Thesis. Université Bordeaux 1, Talence Cédex, France, 2008.

(9) Bhattacharyya, A. J.; Dollé, M.; Maier, J. *Electrochem. Solid-State Lett.* **2004**, *7*, A432.
(10) Balaya, P.; Bhattacharyya, A. J.; Jamnik, J.; Zhukovskii, Yu. F.; Kotomin, E. A.; Maier, J. *J. Power Sources* **2006**, *159*, 171.
(11) Fenton, D. E.; Parker, J. M.; Wright, P. V. *Polymer* **1973**, *14*, 589.
(12) Shriver, D. F.; Bruce, P. G. In *Solid State Electrochemistry*; Bruce, P. G., Ed.; Cambridge University Press: New York, 1995; p 95.
(13) Gray, F. M.; Armand, M. In *Handbook of Battery Materials*; Besenhard, J. O., Ed.; Wiley-VCH: Weinheim, Germany, 1999; p 499.
(14) Bhattacharyya, A. J.; Fleig, J.; Guo, Y.-G.; Maier, J. *Adv. Mater.* **2005**, *17*, 2630.
(15) Croce, F.; Appetecchi, G. B.; Persi, L.; Scrosati, B. *Nature* **1998**, *394*, 456.
(16) Croce, F.; Settimi, L.; Scrosati, B. *Electrochem. Commun.* **2006**, *8*, 364.
(17) Appetecchi, G. B.; Aihara, Y.; Scrosati, B. *Solid State Ionics* **2004**, *170*, 63.
(18) Zaghib, K.; Charest, P.; Guerfi, A.; Shim, J.; Perrier, M.; Striebel, K. *J. Power Sources* **2005**, *146*, 380.
(19) Patel, M.; Chandrappa, K. G.; Bhattacharyya, A. J. *Electrochim. Acta* **2008**, *54*, 209.
(20) Patel, M.; Bhattacharyya, A. J. *Electrochem. Commun.* **2008**, *10*, 1912.
(21) Maier, J. *Prog. Solid State Chem.* **1995**, *23*, 171.
(22) Jarosik, A.; Kaskhedikar, N.; Traub, U.; Bunde, A.; Maier, J. Conductivity and Stability of Particle Networks in Liquids. *International Workshop on Fundamentals of Lithium-based Batteries*, Tegernsee, Germany, November 23−28, 2008.
(23) *Technical Bulletin Fine Particles No. 11: Basic Characteristics of AEROSIL Fumed Silica*. Degussa Corporation, **2003**.
(24) Raghavan, S. R.; Riley, M. W.; Fedkiw, P. S.; Khan, S. A. *Chem. Mater.* **1998**, *10*, 244.
(25) Beck, J. S.; Vartuli, J. C.; Roth, W. J.; Leonowicz, M. E.; Kresge, C. T.; Schmitt, K. D.; Chu, C. T. W.; Olson, D. H.; Sheppard, E. W.; McCullen, S. B.; Higgins, J. B.; Schlenker, J. L. *J. Am. Chem. Soc.* **1992**, *114*, 10834.
(26) Bunde, A.; Dieterich, W. *J. Electrochem. Soc.* **2000**, *5*, 81.
(27) Bunde, A.; Dieterich, W.; Roman, H. E. *Phys. Rev. Lett.* **1985**, *55*, 5.
(28) Reed, J. S. *Principles of Ceramics Processing*, 2nd ed.; John Wiley & Sons, Inc.: New York, 1995; p 152.
(29) Barthel, J.; Gores, H. J. In *Handbook of Battery Materials*; Besenhard, J. O., Ed.; Wiley-VCH: Weinheim, Germany, 1999; p 457.
(30) Macosko, C. W. *Rheology: Principles, Measurements and Applications*; VCH Publishers: New York, 1994.
(31) Raghavan, S. R.; Walls, H. J.; Khan, S. A. *Langmuir* **2000**, *16*, 7920.
(32) Russel, W. B. *Powder Technol.* **1987**, *51*, 15.
(33) Atkins, D. T.; Ninham, B. W. *Colloids Surf., A* **1997**, *129*, 23.
(34) Moreira, A. G.; Netz, R. *Phys. Rev. Lett.* **2001**, *87*, 078301.
(35) Khan, S. A.; Zoeller, N. J. *J. Rheol.* **1993**, *37*, 1225.
(36) Korn, M.; Killmann, E.; Eisenlauer, J. *J. Colloid Interface Sci.* **1980**, *76*, 7.
(37) Kiraly, Z.; Turi, L.; Dekany, I.; Bean, K.; Vincent, B. *Colloid Polym. Sci.* **1996**, *274*, 779.
(38) Ketelson, H. A.; Pelton, R.; Brook, M. A. *Langmuir* **1996**, *12*, 1134.
(39) Depasse, J. *J. Colloid Interface Sci.* **1997**, *194*, 260.
(40) Israelachvili, J. *Intermolecular and Surface Forces*; 2nd ed.; Academic Press: San Diego, CA, 1991.
(41) The Hamaker constant (A_{eff}) is given by the equation $A_{\mathrm{eff}} = (3/4)kT[(\epsilon_m-\epsilon_\delta)^2/(\epsilon_m+\epsilon_\delta)^2] + (3h\nu_e/16\sqrt{2})[(n_m^2-n_\delta^2)^2/(n_m^2+n_\delta^2)^{3/2}]$. Here, ϵ is the dielectric constant and n is refractive index. Subscript δ refers to the functionalized group layer, and m refers to continuous medium; k = Boltzmann constant, T = absolute temperature, h = Planck's constant, and $\nu_e = 3 \times 10^{15}\ s^{-1}$. For OA300, considering the value of *n*-octane, $\epsilon = 1.95$ and $n = 1.387$ at 20 °C. For MA300, considering the value of methane, $\epsilon = 1.00079$[42] and $n \cong 1.00029$ at 27 °C. For ethylene glycol, $\epsilon = 37.7$ and $n = 1.431$ at 20 °C.
(42) Younglove, B. A.; Ely, J. F. *J. Phys. Chem. Ref. Data* **1987**, *16*, no 4.
(43) Website of Sigma Aldrich: http://www.sigmaaldrich.com/catalog/. Product number 85978 (ethylene glycol).
(44) Raghavan, S. R.; Hou, J.; Baker, G. L.; Khan, S. A. *Langmuir* **2000**, *16*, 1066.
(45) Zeigler, R. C.; Maciel, G. E. *J. Am. Chem. Soc.* **1991**, *113*, 6349.
(46) Cosgrove, T.; Crowley, T. L.; Ryan, K.; Webster, J. R. P. *Colloids Surf.* **1990**, *51*, 255.
(47) Ingersent, K.; Klein, J.; Pincus, P. *Macromolecules* **1986**, *19*, 1374.
(48) Zhulina, E. B.; Borisov, O. V.; Priamitsyn, V. A. *J. Colloid Interface Sci.* **1990**, *137*, 495.
(49) Besseling, N. A. M. *Langmuir* **1997**, *13*, 2113.
(50) Forsman, J.; Woodward, C. E.; Jönsson, B. *J. Colloid Interface Sci.* **1997**, *195*, 262.
(51) Kiraly, Z.; Turi, L.; Dekany, I.; Bean, K.; Vincent, B. *Colloid Polym. Sci.* **1996**, *274*, 779.
(52) Ketelson, H. A.; Pelton, R.; Brook, M. A. *Langmuir* **1996**, *12*, 1134.

JP810761E